A R C H I V E O F M E C H A N I C A L E N G I N E E R I N G

VOL. LXIII 2016 Number 1

10.1515/meceng-2016-0002

Key words: coil spring – rubber, suspension, railway vehicle, stiffness, damping

MĂDĂLINA DUMITRIU *

A NONLINEAR MODEL OF MIX COIL SPRING – RUBBER FOR VERTICAL SUSPENSION OF RAILWAY VEHICLE

The paper focuses on a nonlinear model to represent the mechanical behaviour of a mix coil spring – rubber used in the secondary suspension of passenger rail vehicles. The principle of the model relies on overlapping of the forces corresponding to three components – the elastic component, the viscous component and the dry friction component. The model has two sources on non-linearity, in the elastic force and the friction force, respectively. The main attributes of the model are made visible by its response to an imposed displacement-type harmonic excitation. The results thus obtained from the applications of numerical simulation show a series of basic properties of the model, namely the dependence on amplitude and the excitation frequency of the model response, as well as of its stiffness and damping.

1. Introduction

The simulation of dynamics in railway vehicles represents a basic tool in research that one uses since the designing stage in order to estimate the dynamic behaviour of the railway vehicle and to optimize its dynamic performance and to investigate the problems arising during exploitation [1, 2]. In recent years, the specifications on the homologation of the railway vehicles in terms of the dynamic behaviour for safety, track fatigue and ride quality [3, 4] have been added to a series of requirements to complete the tests based on computational models of the vehicle and virtual simulations, thus regulating the so-called – "virtual homologation" procedure.

The potential and success of vehicle dynamic simulations greatly depend on how the mechanical properties of the vehicle in general, and its components, in particular, are modelled [5]. The above applications require a high degree of reliability and trust of in the applied models, since any significant

* *Department of Railway Vehicles, University Politehnica of Bucharest, Bucharest, Romania; E-mail: madalinadumitriu@yahoo.com*

deviation of them from the behaviour of the real vehicle would involve the need to refit the vehicle during the advanced designing stage or even in the homologation process, given the fact that some of the issues under study are critical in terms of safety [6].

Even though the railway vehicles contain numerous components, it is important to have the representation of the mechanical properties of the main components for the vehicle – track dynamic simulations. The suspension components hold an important place in the dynamic behaviour of the railway vehicles and, hence, the adopted models are critical for the precision of the vehicle multibody models [5-7].

The principal suspension components in the railway vehicles are the springs (coil springs, leaf spring, rubber springs, rubber-metal springs, plate spring, ring spring, air spring, etc.) and the dampers. The traction rods, bump stops, antiroll bars, trailing arms, linkages, etc. also belong to this group of components. In recent years, the modelling of the diverse suspension components has been the topic of research works and updated reviews of them can be found in the review literature [5, 6, 8].

The point in question of this paper aims at the mix metal spring – rubber suspension components, as they can be found in both the primary and secondary suspensions of the railway vehicles. In these suspension components the metal springs operate in parallel with the rubber elements.

The paper herein introduces a mix coil spring – rubber used in the secondary suspension of the passenger railway vehicles. The model of this suspension component is developed on the basis of a non-linear dynamic rubber spring model, to be found in the review literature [11], which best reflects the mechanical behaviour of rubber suspension components in rail vehicle dynamics and also provides a very good agreement between the theoretical and experimental results. As a principle, the model in this paper, similar with the initial one, relies on overlapping of three component forces, working in parallel – the elastic force, viscous force and friction force, where each of them contributes to the total force of deformation of the elastic system. Unlike the initial model, described by five parameters, the model recommended here has six parameters, coming from the representation of the elastic component by an elastic element with variable step stiffness. Thus, the model has two sources of non-linearity – one from the component of the friction force while the other one caused by the elastic force component.

The main properties of the model, namely the dependence of its response on the excitation amplitude and frequency, are pointed out at by means of certain applications of numerical simulation, developed via the Matlab programming environment. Similarly, the influence of the excitation parameters on the model stiffness and damping will be examined.

2. The static characteristic of the mix coil spring-rubber

Figure 1 shows a mix coil spring – rubber used in the secondary suspension of the Y 32R bogie which certain passenger rail vehicles are fitted with. This combination of steel coil spring and rubber benefits from a high stiffness in the vertical direction and a low stiffness in the transversal one.

The static characteristic of the mix in the vertical direction is featured in Fig. 2. This characteristic is noticed to be of a non-linear type with stepwise variation of stiffness. The stiffness of the mix increases along with the applied loading, due to the rubber deformation. For a certain loading, the rubber element enters between the coils of the steel spring and blocks it from moving in the vertical direction, after a certain degree of deformation.

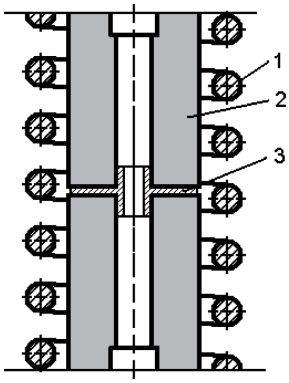

Fig. 1. Mix coil spring – rubber: 1. coil spring; 2. rubber; 3. intermediary element

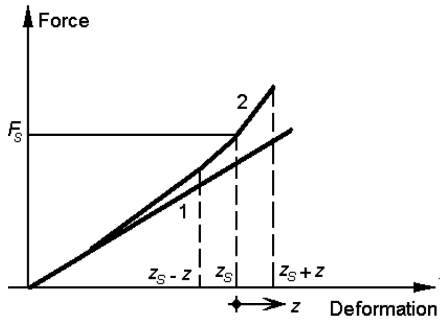

Fig. 2. The static characteristic of the mix: 1. the characteristic of the steel spring; 2. the characteristic of the coil spring + rubber

From the perspective of the simulation in the dynamic behaviour of the railway vehicle, what holds the attention is how the mix behaves when it has a deformation z around the point z_s, corresponding to the static load F_s.

In dynamic behaviour, the properties of the rubber and of the non-linear elastic element trigger an asymmetric hysteresis cycle, which is also present at a very low frequency.

3. The non-linear model of the mix coil spring-rubber

The model of the mix coil spring-rubber presented in this section is based on the Berg model, which very well expresses mechanical behaviour of rubber suspension components in rail vehicle dynamics [9-11]. It should be noticed that the Berg model provides a good consistence between the theoretical and experimental results and represents a reasonable compromise between accuracy and computational effort.

As a principle, the Berg model is a dimensional one, based on the overlapping of three component forces working in parallel, where each of them contributes to the total deformation force of the rubber spring (Fig. 3) [9]. They include the component of the elastic force (F_e), the viscous force (F_v) and the dry friction component (F_f). The elastic force component is linear and models the rubber elasticity property. When introducing the viscous force, the increase in stiffness triggers a similar frequency response, as well as the rate-dependent hysteresis. The inclusion of a friction force means an increased stiffness at small displacement amplitudes as well as rate-independent hysteresis.

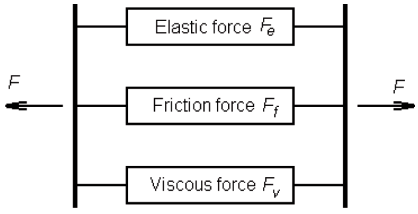

Fig. 3. Model principle to represent the rubber springs [9]

The model described in this paper, suggested for representing the mix coil spring-rubber as described in the previous section, is featured in Fig. 4. The model, as one can notice, consists of the same three components operating in parallel, as in the Berg model. The elastic force component is thus described by an elastic element that has a variable stiffness k_e, unlike the Berg model. It includes both the elastic force in the coil spring and the other one in the rubber element. As for the viscous force component, this is represented by a Maxwell system containing an element of viscous damping of constant c_v in series with an elastic element of stiffness k_v.

We ultimately have the component of the friction force, whose modelling is based on Coulomb's dry friction theory ($F_f = \mu N$, where μ is the friction

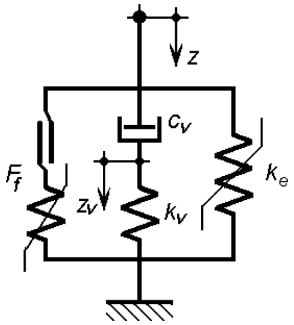

Fig. 4. Model for mix coil spring – rubber

coefficient and N – the normal load). As a principle, to avoid the issues emerging during the numerical simulations due to the fact that Coulomb model is non-smooth, multi-valued and non-differentiable (see the force-displacement curve – Fig. 5, a), a linear spring in series with a friction slider is used (Fig. 6) [6]. The result will be the force-displacement curve, shown in Fig. 5b. The present friction model can be seen as a 'smooth Coulomb friction force' [9-11]. Here, (see Fig. 4) the spring in series with the friction slider has a non-linear characteristic.

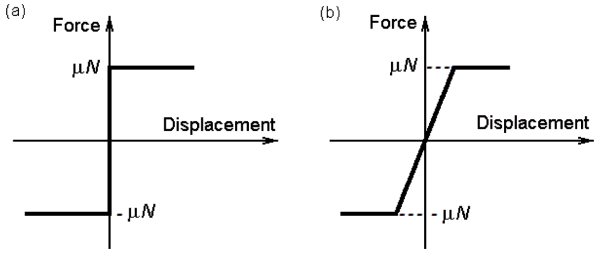

Fig. 5. Force–displacement curve: a) Coulomb friction model; b) Coulomb model with spring in series

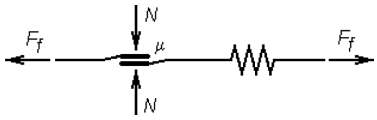

Fig. 6. Friction element with spring in series

An observation can be made that the non-linearity of the model results, on the one hand, from the elastic force component developed in the mix coil spring–rubber and, on the other hand, from the component of friction force occurring in the rubber element.

For a displacement z in relation to the equilibrium position of the system under the action of the static force, the total force F is equal to the sum of those three forces appearing in the components of the model

$$F = F_e + F_v + F_f. \tag{1}$$

The elastic force is calculated as a function of the direction of the displacement z, while considering the variation in the stiffness of the elastic mix

$$F_{e1} = k_{e1}z, \qquad \text{for} \quad z > 0; \tag{2}$$

$$F_{e2} = k_{e2}z, \qquad \text{for} \quad z \leq 0, \tag{3}$$

with $k_{e1} > k_{e2}$.

The viscous force is determined as follows

$$F_v = c_v(\dot{z} - \dot{z}_v) = k_v z_v. \tag{4}$$

In this model, the friction model depends on the displacement z of the system, as well as on the reference state, defined by the coordinates of the turning point in the cycle running, (z_r, F_{fr}) [9]. For instance, Fig. 7 shows three segments of a cycle, denoted with (a), (b) and (c). The segment (a) is the one to start with and the corresponding reference state is defined by the null conditions $(z_{ra}, F_{fra}) = (0, 0)$. Further on, when climbing on the segment (a), the point (z_{rb}, F_{frb}) is reached when the cycle running is reversed and the segment (b) originates. Thus, the reference state for this segment is the point (z_{rb}, F_{frb}). The segment (b) ends in the point (z_{rc}, F_{frc}), where there is another reversal of the cycle running, since the segment (c) begins. As a result, this point becomes the reference state for the segment (c).

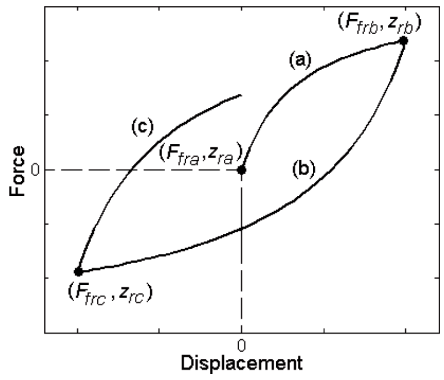

Fig. 7. Explanatory graph for the steady states of the friction force

Besides the reference state, two more parameters of the friction force component model are defined, namely the maximum friction force $F_{f\max}$

and the displacement z_2 for which the friction force is half the value of the maximum friction force $F_f = F_{f\max}/2$, when starting from the initial reference state $(z_{ra}, F_{fra}) = (0, 0)$ and reaching $z = z_2$.

The friction force is defined in relation to the reference state, as follows:

– for $z = z_r$

$$F_f = F_{fr}; \tag{5}$$

– for $z > z_r$ – ascendant segment

$$F_f = F_{fr} + \frac{z - z_r}{z_2(1-\alpha) + (z - z_r)}(F_{f\max} - F_{fr}); \tag{6}$$

– for $z < z_r$ – descendent segment

$$F_f = F_{fr} + \frac{z - z_r}{z_2(1+\alpha) - (z - z_r)}(F_{f\max} + F_{fr}), \tag{7}$$

where the parameter α is given by the reference force-maximum friction force relation,

$$\alpha = \frac{F_{fr}}{F_{f\max}}, \tag{8}$$

and its values range from –1 to 1.

Should $z_2 = 0$ is considered in the equations (6) and (7), then the friction force is constant and will have the maximum value $F_{f\max}$, namely:

– for $z > z_r$

$$F_f = F_{f\max}; \tag{9}$$

– for $z < z_r$

$$F_f = -F_{f\max} \tag{10}$$

$$\text{or,} \qquad F_f = F_{f\max} sgn(\dot{z}), \tag{11}$$

which proves the fact that the friction force is of a Coulomb type.

4. The model response to a harmonic excitation

In order to describe the dynamic behaviour of the model herein, the study will focus on its response to an imposed displacement of harmonic type of amplitude z_o and circular excitation frequency ω,

$$z = z_o \sin \omega t. \tag{12}$$

Figure 8 features the stationary response of a hysteretic mechanical system to a harmonic input, under the form of a force-displacement cycle (z, F),

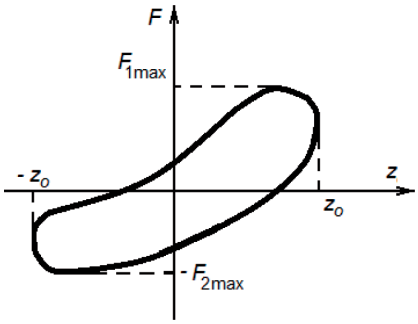

Fig. 8. Steady-state response

asymmetric in relation to the steady state. Such a cycle can be described by two parameters: stiffness and damping.

The stiffness of the system is defined as the relation between the amplitude of the total force (F_o) calculated as an average of the maximum forces of the cycle ($F_{1\,\max}$ and $F_{2\,\max}$) and the amplitude of the displacement (z_o)

$$S = \frac{F_o}{z_o}, \tag{13}$$

where $F_o = (F_{1\,\max} + F_{2\,\max})/2$ (Fig. 9a).

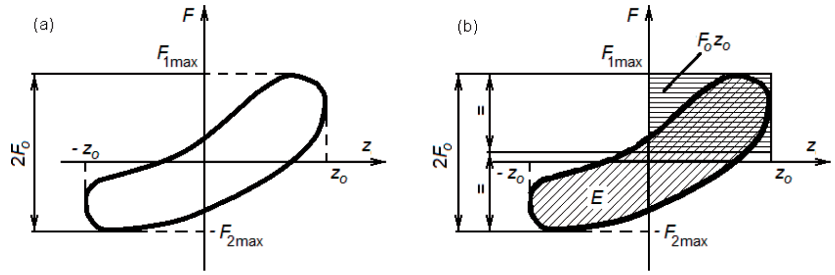

Fig. 9. Definition of characteristics of steady-state response: a) stiffness; b) damping

The damping of the system is the ratio between the energy dissipated per cycle and the product between the force amplitude and the displacement amplitude

$$D = \frac{E}{F_o z_o}, \tag{14}$$

which comes back to the ratio between the areas displayed in Fig. 9b.

The calculation of the two above-defined coefficients requires knowing the amplitude of the total force and of the energy dissipated per cycle. Hence, it is necessary to calculate the amplitude of each component force in the model and the loss of the corresponding energy. To do so for the elastic

force, the variation of the mix stiffness will be taken into account, which triggers the below maximum forces per cycle:

$$F_{e1\,\max} = k_{e1} z_o, \qquad \text{for} \quad z > 0; \tag{15}$$

$$F_{e2\,\max} = k_{e2} z_o, \qquad \text{for} \quad z \leq 0. \tag{16}$$

As a result, the amplitude of the elastic force is as such

$$F_{eo} = \frac{F_{e1\,\max} + F_{e2\,\max}}{2}. \tag{17}$$

Further on, it is possible to have the value of the stiffness S_e of the elastic element to the harmonic excitation of amplitude z_o,

$$S_e = \frac{F_{eo}}{z_o}. \tag{18}$$

As for the loss of the energy per cycle, this is zero ($E_e = 0$) and, hence, the damping written as

$$D_e = \frac{E_e}{F_{eo} z_o}, \tag{19}$$

is also zero.

The response of the elastic element model is noticed to be independent on frequency and hysteresis.

In a steady-state harmonic behaviour, the outputs of Maxwell system are

$$F_v(t) = F_{vo} \cos(\omega t + \varphi_F); \tag{20}$$

$$z_v(t) = z_{vo} \cos(\omega t + \varphi_z), \tag{21}$$

where F_{vo} is the amplitude of the force, z_{vo} – amplitude of the displacement and φ_F and φ_z are the corresponding phase differences.

The complex values associated with the real ones are introduced:

$$\bar{F}_v(t) = \bar{F}_v \mathrm{e}^{\mathrm{i}\omega t}, \quad \bar{z}_v(t) = \bar{z}_v \mathrm{e}^{\mathrm{i}\omega t}, \quad \bar{z}(t) = \bar{z}_o \mathrm{e}^{\mathrm{i}\omega t}, \tag{22}$$

with the complex amplitudes

$$\bar{F}_v = F_{vo} \mathrm{e}^{\mathrm{i}\varphi_F}, \quad \bar{z}_v = z_v \mathrm{e}^{\mathrm{i}\varphi_z}, \quad \bar{z} = z_o, \tag{23}$$

where $\mathrm{i}^2 = -1$.

The relation (4) becomes an algebraic equation

$$\bar{F}_v = \mathrm{i}\omega c_v (\bar{z} - \bar{z}_v) = k_v \bar{z}_v, \tag{24}$$

from which the complex amplitude of the viscous force derives

$$\bar{F}_v = \frac{\mathrm{i}\omega c_v}{1 + \mathrm{i}\omega c_v/k_v}\bar{z} = k_v z_o \left(\frac{(\omega c_v/k_v)^2}{1 + (\omega c_v/k_v)^2} + \mathrm{i}\frac{\omega c_v/k_v}{1 + (\omega c_v/k_v)^2} \right). \tag{25}$$

From the latest equation, the real and the imaginary parts of the complex amplitude in the viscous force will result

$$F_{voRe} = \frac{(\omega c_v/k_v)^2}{1 + (\omega c_v/k_v)^2} k_v z_o; \tag{26}$$

$$F_{voIm} = \frac{1}{1 + (\omega c_v/k_v)^2} \omega c_v z_o, \tag{27}$$

as well as the amplitude of the viscous force

$$F_{vo} = \left|\bar{F}_v\right| = \frac{\omega c_v}{\sqrt{1 + (\omega c_v/k_v)^2}} z_o. \tag{28}$$

In order to calculate the energy dissipated per cycle, it is required to write the equation of Maxwell cycle. For this purpose, the starting point is the viscous force relation (20), which shows as below

$$F_v(t) = F_{vo}\cos(\omega t + \varphi_F) = F_{vo}\cos\varphi_F \cos\omega t - F_{vo}\sin\varphi_F \sin\omega t, \tag{29}$$

where, corresponding to relation (25), we have

$$F_{vo}\cos\varphi_F = k_v z_o \frac{(\omega c_v/k_v)^2}{1 + (\omega c_v/k_v)^2}; \quad F_{vo}\sin\varphi_F = k_v z_o \frac{\omega c_v/k_v}{1 + (\omega c_v/k_v)^2}, \tag{30}$$

Similarly, the equations below come from relation (12)

$$\cos\omega t = \frac{z}{z_o}; \quad \sin\omega t = \pm\sqrt{1 - \left(\frac{z}{z_o}\right)^2}. \tag{31}$$

The equation of Maxwell model cycle is further derived

$$F_v = F_{v1,2} = k_v z_o \frac{(\omega c_v/k_v)^2}{1 + (\omega c_v/k_v)^2} \frac{z}{z_o} \pm k_v z_o \frac{\omega c_v/k_v}{1 + (\omega c_v/k_v)^2} \sqrt{1 - \left(\frac{z}{z_o}\right)^2}. \tag{32}$$

Hereinafter, the energy dissipated per cycle can be calculated

$$E_v = \int_{-z_o}^{z_o} (F_{v1} - F_{v2})dz = \frac{\pi\omega c_v}{1 + (\omega c_v/k_v)^2} z_o^2, \tag{33}$$

which can be noticed to have a maximum value for $\omega = k_v/c_v$, with

$$E_{v\max} = 0.5\pi k_v z_o^2. \tag{34}$$

The stiffness and damping for the viscous component of the model are

$$S_v = \frac{F_{vo}}{z_o} = \frac{\omega c_v}{\sqrt{1 + (\omega c_v/k_v)^2}}; \tag{35}$$

$$D_v = \frac{E_v}{F_{vo} z_o} = \frac{\pi \omega c_v}{\sqrt{1 + (\omega c_v/k_v)^2}}. \tag{36}$$

The representation of the first friction force – displacement for harmonic excitation cycle is featured in Fig. 7. For the segment (a), the friction force writes as

$$F_f = \frac{z}{z_2 + z} F_{f\max}, \tag{37}$$

that comes from equation (6) where $F_{fr} = 0$, $z_r = 0$ and, consequently, $\alpha = 0$.

It is a sure fact that for $z = z_2$, the friction force reaches a half value of the maximum friction force $F_{f\max}$. On the other hand, for $z = z_o$, the force corresponding to the limit of the segment (a) is obtained, which becomes the reference value for the segment (b)

$$F_{frb} = \frac{z_o}{z_2 + z_o} F_{f\max}. \tag{38}$$

What can be confirmed is that the value of F_{frb} is lower than the maximum friction force, but with a gradual increase in the excitation amplitude, the force F_{frb} tends to reach to $F_{f\max}$.

For the segment (b), the friction force comes from relation (7) where $F_{fr} = F_{frb}$, $z_r = z_o$ and $\alpha = F_{frb}/F_{f\max} = z_o/(z_2 + z_o)$

$$F_f = F_{f\max} \frac{z_o}{z_2 + z_o} \left[1 + \frac{(z - z_o)(z_2 + z_o)}{z_2(z_2 + 2z_o) - (z_2 + z_o)(z - z_o)} \frac{z_2 + 2z_o}{z_o} \right]. \tag{39}$$

When $z = -z_o$, at the end of the segment (b), the friction force will take the reference value for segment (c)

$$F_{frc} = -F_{f\max} \frac{z_o}{z_2 + z_o} \frac{(z_2 + z_o)^2 + z_o^2}{(z_2 + z_o)^2 + z_o^2 + 2z_2 z_o} \tag{40}$$

and the observation is that this force is not equal (in module) with the other reference value (see 38). In other words, the cycle is not symmetrical.

The same conclusion will be drawn – the fact that the cycle is not symmetrical – when the calculations are completed for the segment (c). Moreover, the limit value of the segment (c) does not coincide with the one of segment (a). Nevertheless, after more successive cycles, the friction force – displacement characteristic becomes steady, as shown in Fig. 10. Additionally, the stabilized characteristic is symmetrical, as hereinafter demonstrated.

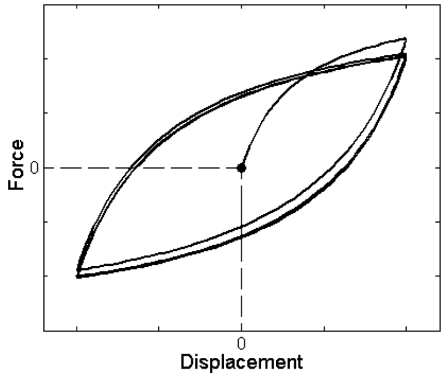

Fig. 10. Stabilization of the friction force – displacement characteristic

While considering the two reference states of the friction force – displacement stabilized characteristic (see Fig. 11) with (z_o,F_{fr1}), and (– z_o, F_{fr2}), the relations (6) and (7) become:

– for $z > z_o$, the ascendant segment

$$F_f = F_{fr2} + \frac{z + z_o}{z_2(1 - F_{fr2}/F_{f\max}) + (z + z_o)}(F_{f\max} - F_{fr2}); \tag{41}$$

– for $z < z_o$ – the descendent segment

$$F_f = F_{fr1} + \frac{z - z_o}{z_2(1 + F_{fr1}/F_{f\max}) - (z - z_o)}(F_{f\max} + F_{fr1}), \tag{42}$$

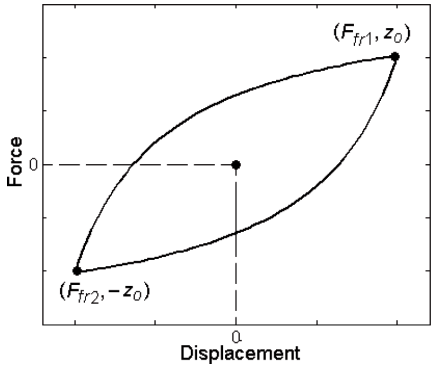

Fig. 11. Explanatory graph for the calculation of the friction force – displacement stabilized cycle

provided that the relation (6) has $\alpha = F_{fr2}/F_{f\max}$, and in (7), $\alpha = F_{fr1}/F_{f\max}$.

In addition, for the ascendant segment $z = z_o$ and, hence, $F_f = F_{fr1}$, whereas for the descendent segment, $z = -z_o$, meaning $F_f = F_{fr2}$. As a result, the following relations are derived

$$F_{fr1} = F_{fr2} + \frac{2z_o}{z_2(1 - F_{fr2}/F_{f\max}) + 2z_o}(F_{f\max} - F_{fr2}); \tag{43}$$

$$F_{fr2} = F_{fr1} - \frac{2z_o}{z_2(1 + F_{fr1}/F_{f\max}) + 2z_o}(F_{f\max} + F_{fr1}). \tag{44}$$

The two equations above will infer

$$F_{fr1} = -F_{fr2} = F_{fo}, \tag{45}$$

which proves the symmetry of the friction force – displacement stabilized cycle.

This cycle is in the form of

$$F_{f1} = F_{f\max}\left[-\alpha_o + \frac{z + z_o}{z_2(1 + \alpha_o) + (z + z_o)}(1 + \alpha_o)\right]; \tag{46}$$

$$F_{f2} = F_{f\max}\left[\alpha_o + \frac{z - z_o}{z_2(1 + \alpha_o) - (z - z_o)}(1 + \alpha_o)\right], \tag{47}$$

where $\alpha_o = F_{fo}/F_{f\max}$.

The amplitude of the friction force in the stabilized cycle will be further calculated (for $z = z_o$, $F_{f1} = F_{fo}$ or for $z = -z_o$, $F_{f2} = -F_{fo}$)

$$F_{fo} = \frac{F_{f\max}}{2z_2}\left[\sqrt{(z_2^2 + z_o^2 + 6z_2z_o)} - z_2 - z_o\right]. \tag{48}$$

The loss of energy per cycle comes from

$$E_f = \int_{-z_o}^{z_o}(F_{f1} - F_{f2})\mathrm{d}z = 2F_{f\max}\left[2z_o - z_2(1 + \alpha_o)^2 \ln\frac{z_2(1 + \alpha_o) + 2z_o}{z_2(1 + \alpha_o)}\right]. \tag{49}$$

The equation for the stiffness in the friction model at a harmonic excitation is

$$S_f = \frac{F_{f_o}}{z_o} = \frac{F_{f\max}}{2z_2z_o}\left[\sqrt{(z_2^2 + z_o^2 + 6z_2z_o)} - z_2 - z_o\right] \tag{50}$$

and the damping results from

$$D_f = \frac{E_f}{F_{fo}z_o} = \frac{2}{\alpha_o z_o}\left[2z_o - z_2(1 + \alpha_o)^2 \ln\frac{z_2(1 + \alpha_o) + 2z_o}{z_2(1 + \alpha_o)}\right]. \tag{51}$$

To calculate the amplitude of the force developed in the mix coil spring – rubber, there will be considered that the amplitude of the viscous force has two components in quadrature

$$F_o = \sqrt{\left(F_{eo} + F_{fo} + F_{voRe}\right)^2 + F_{voIm}^2}, \tag{52}$$

where F_{eo} comes from relation (17), F_{voRe} and F_{voIm} is calculated with (26-27), while (48) is applied for F_{fo}.

The energy loss per cycle is calculated by summing up the quantities of energy E_v (33) and E_f (49), namely

$$E = E_v + E_f. \tag{53}$$

Ultimately, the stiffness and damping can be now calculated at a harmonic excitation, using the relations (13) and (14) where F_o and E are replaced, as per in the equations (52) and (53).

5. The results of the numerical simulations

Based on the results derived from the numerical simulations, this section focuses on the basic properties of the model herein, namely its dependence on the amplitude and frequency of the excitation. For this purpose, we have the response of the model to a harmonic excitation of an imposed displacement type. Similarly, there will be an analysis of the manner in which the displacement amplitude and excitation frequency influences the stiffness and damping of the model.

The reference parameters of the model are the following k_{e1} = 660 kN/m, k_{e2} = 540 kN/m, z_2 = 0.2 mm, $F_{f\max}$ = 0.3 kN, k_v = 125 kN/m and c_v = 2 kNs/m.

As for the displacement amplitude, it takes typical values for the secondary suspension of a railway vehicle, namely: medium displacements, 3-15 mm; large displacements, 8-50 mm [9].

Figure 12 features the force – displacement characteristic of the model at a harmonic excitation with the amplitude of 10 mm and frequency from 0.1, 1, 6 and 8 Hz. The first value of the frequency corresponds with a quasi-static excitation, with a slow variation – the period of 10 s, while the other values are very close to the most important natural frequencies of the vehicle, namely the natural frequencies of bounce movement and the natural frequency of the first symmetrical bending mode in the carbody [12]. The diagrams also present the characteristics of those three components of the model, such as the elastic force, friction force and the viscous force. It is

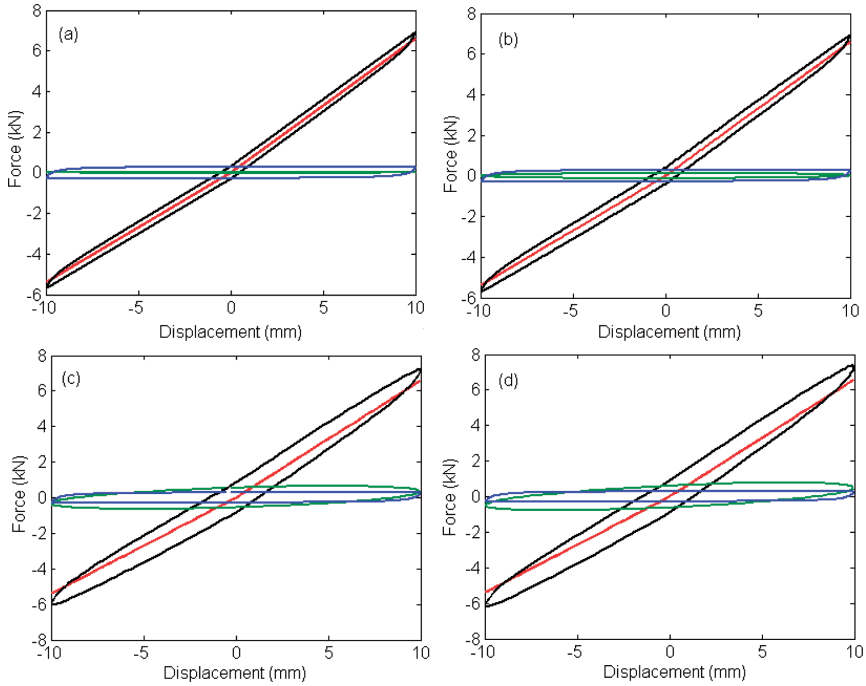

Fig. 12. Influence of the excitation frequency upon the force – displacement characteristic: a) at 0.1 Hz, b) at 1 Hz; c) at 6 Hz; d) at 8 Hz;
— , elastic force (F_e); — , friction force (F_f); — , viscous force (F_v); — , total force (F)

visible that the elastic force does not change with the excitation frequency, maintaining the same amplitude (F_{eo} = 6 kN). This is in the shape of a broken line due to the variation in the stiffness, which is higher for positive displacements and lower for negative displacements. Consequently, the force-displacement characteristic of the model takes the form of a broken loop.

The friction force is also independent from the excitation frequency. Even though the maximum friction force is 0.3 kN, the maximum force effectively reached is 0.288 kN. For the 10 mm displacement, the stiffness corresponding to the friction component in the model is 28.867 kN/m, and the damping is 3.524 kNs/m.

The amplitude of the viscous force increases along the frequency, as it is a function of velocity. At 0.1 Hz, the influence of this force is not significant (F_{vo} = 0.012 kN), it though becomes more visible at 1 Hz (F_{vo} = = 0.125 kN); at 6 and 8 Hz, this force brings a higher contribution than the friction one (F_{vo} = 0.645 kN and F_{vo} = 0.783 kN). In addition to the rise of the hysteresis, the increase in the excitation frequency will trigger a higher stiffness (Fig. 13a) and smaller damping (Fig. 13b), corresponding to the viscous component in the model.

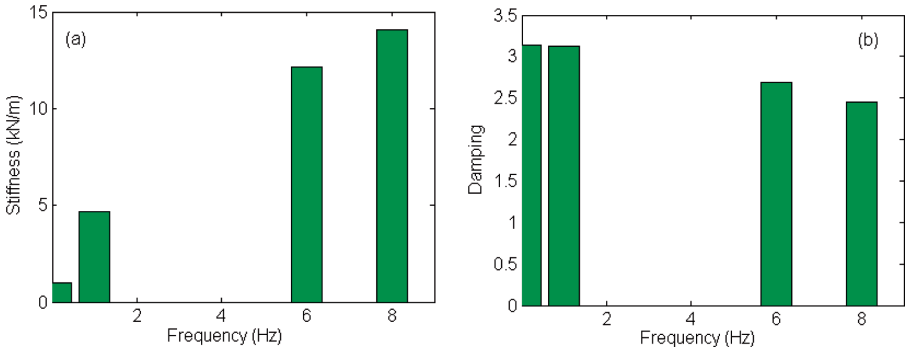

Fig. 13. Influence of the excitation frequency upon the stiffness and damping in the viscous component of the model

Finally, the amplitude of the total force (F_o) can be shown to change along with the frequency. In other words, starting at the value of 6.288 kN, corresponding to the frequency of 0.1 Hz, the force is 6.807 at 8 Hz.

The influence of the excitation amplitude upon the force-displacement characteristic is featured in Fig. 14. Two values of the amplitude are taken into account, namely a medium value of 10 mm and a large value, of 30 mm.

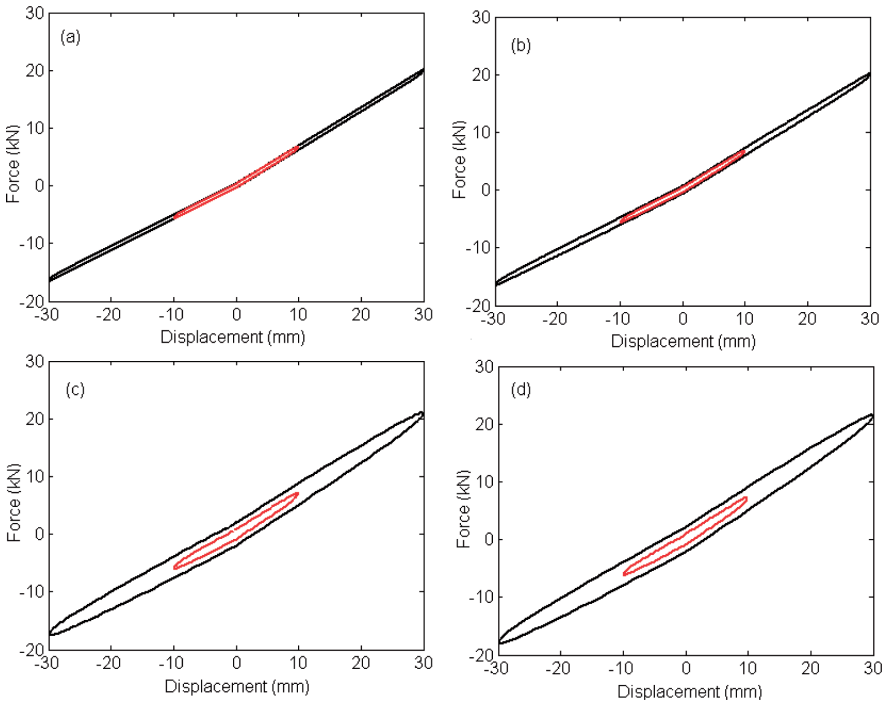

Fig. 14. Influence of the excitation amplitude upon the force-displacement characteristic: a) at 0.1 Hz; b) at 1 Hz; c) at 6 Hz; d) at 8 Hz; — , z_o = 10 mm; — , z_o = 30 mm

Similarly, the correlation with the excitation frequency will be done, while considering the four frequencies in the previous example. The increase of the hysteresis can be noticed, along with the excitation amplitude in all four cases under study. The amplitude of the total force also rises circa 3 times when amplitude goes from 10 mm to 30 mm. For instance, at frequency of 1 Hz, F_o steps up from 6.302 kN to 18.337 kN, and from 6.807 kN to 19.853 kN, for 8 Hz.

Neither the rigidity coming from the viscous force is clearly a function of amplitude – as it is a linear model for it –, nor the rigidity due to the elastic element being dependent on the excitation amplitude, since its rigidity is steady on a semicycle. It is only the friction force a function of the excitation amplitude, which triggers a lower stiffness for higher amplitude. This can be seen in Fig. 15, which depicts how the friction force varies for certain cycles with different amplitudes, of 10 and 30 mm, respectively. Thus, should the cycle is a 10 mm amplitude, then the stiffness coming from the friction force is of 28.867 kN/m, which lowers to 9.869 kN/m, for a 30 mm amplitude cycle.

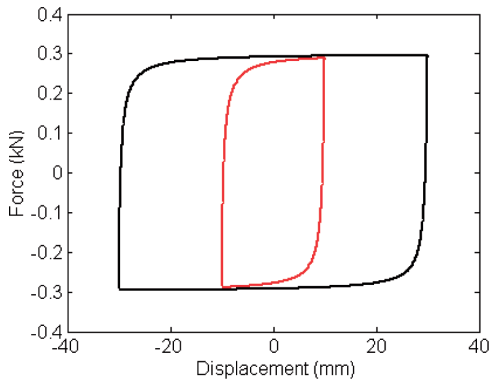

Fig. 15. Influence of the excitation amplitude upon the friction force:
— , z_o = 10 mm; — , z_o = 30 mm

Further on, based on the diagrams in Fig. 16 and Fig. 17, the influence of the excitation amplitude and frequency upon the model stiffness and damping is examined. The stiffness is noticed to decrease when the excitation amplitude increases, irrespective of frequency. Thus, with amplitude going from 6 mm to 50 mm, at frequency of 1 Hz, the stiffness lowers from 0.648 kN/mm to 0.607 kN/mm. Should the excitation frequency is 6 Hz, the decline takes place from 0.682 kN/mm to 0.641 kN/mm. For 8 Hz, stiffness comes from 0.698 kN/mm to 0.658 kN/mm. The decrease in stiffness is more important up to a certain value of displacement (circa 22 mm), after which variation is much smaller. As for the frequency dependence, stiffness rises along with

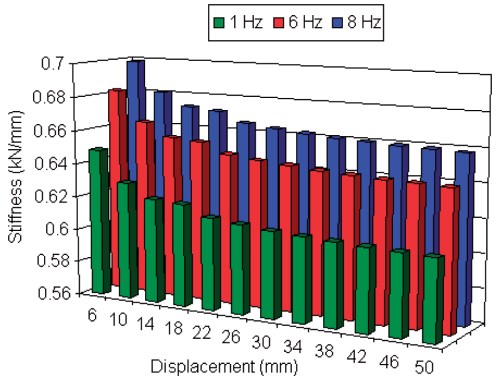

Fig. 16. Influence of the excitation amplitude and frequency upon stiffness

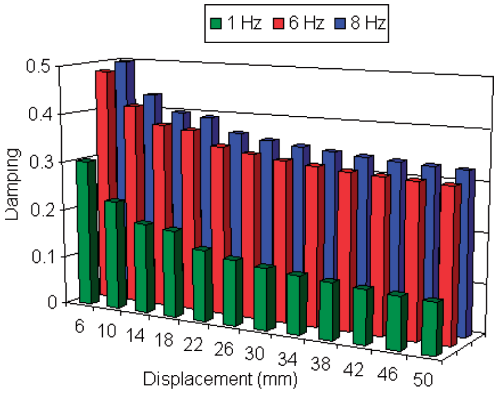

Fig. 17. Influence of the excitation amplitude and frequency upon damping

frequency. For instance, there is S = 0.630 kN/mm, at 1 Hz, for a 10 mm displacement; S = 0.664 kN/mm, at 6 Hz and S = 0.680 kN/mm, for frequency of 8 Hz.

The damping shows similar characteristics as those of the stiffness. On the one hand, it is about a lower damping for increased excitation amplitude and, on the other hand, a smaller damping for a higher excitation frequency. Should the excitation amplitude comes from 6 to 50 mm, at 1 Hz, damping will lower 3 times. Further, damping reduces by 1.58 times at 6 Hz or by 1.52 times at 8 Hz. These examples confirm the fact that the damping reduction rate along with displacement is higher for small frequencies. For a 10 mm displacement, it can be proven that a frequency increase from 1 to 6 Hz triggers an increase from 0.22 to 0.41 in the damping, and then to 0.43, should the frequency keeps going up to 8 Hz.

6. Conclusions

The paper herein introduces a non-linear model for the representation of a mix coil spring – rubber, used in the secondary suspension of the railway vehicles. The basic principle of the model consists in the overlapping of a non-linear elastic component that models the characteristic of elasticity as a function of the loading in the mix, of a viscous component that helps describe the dependence of the rigidity of the rubber element on the frequency, as well as the hysteresis dependence rate and the friction component with a non-linear characteristic for which an increased stiffness of the rubber element at small displacement amplitudes as well as rate-independent hysteresis are considered.

The results of the numerical simulations derived from the model implementation in the computer package Matlab highlight a series of its properties. On the one hand, it is about the dependence of the model response to the amplitude and frequency of a harmonic excitation of an imposed displacement type. It has been validated that both an increase in the excitation frequency and the displacement amplitude trigger a higher hysteresis in the force – displacement characteristic. There are visible a higher stiffness and a lower damping corresponding to the viscous component of the model when frequency increases. Similarly, the dependence of the friction force on the amplitude makes this force-related stiffness decrease along with the increase in the amplitude.

On the other hand, it is shown the influence of the excitation amplitude and frequency upon stiffness and damping in the model. Generally speaking, both parameters exhibit comparable characteristics – they are both smaller when the excitation amplitude is higher and increase along with a growth in frequency. It is worth mentioning that a decrease in stiffness and damping when amplitude rises manifests for any excitation frequency. Likewise, an increase in stiffness and damping for a higher frequency occurs at any excitation amplitude. Another observation to make is that the decrease in stiffness is more important within the interval corresponding to the medium displacements and that the damping-displacement decrease rate is higher at low excitation frequencies.

Manuscript received by Editorial Board, July 13, 2015;
final version, December 04, 2015.

REFERENCES

[1] Evans J., Berg M.: Challenges in simulation of rail vehicle dynamics, Vehicle System Dynamics, 2009, Vol. 47, pp. 1023-1048.

[2] Schupp G.: Simulation of railway vehicles: Necessities and applications, Mechanics Based Design of Structures and Machines, 2003, Vol. 31, Iss. 3, pp. 297-314.
[3] UIC 518 Leaflet – 4th edition – Sept. 2009: Testing and approval of railway vehicles from the point of view of their dynamic behaviour – Safety – Track fatigue – Running behaviour.
[4] EN 14363 – 2013: Railway applications – Testing and Simulation for the acceptance of running characteristics of railway vehicles – Running behaviour and stationary tests.
[5] Polach O., Berg M., Iwnicki S.: Simulation. In Handbook of Railway Vehicle Dynamics, Chapter 12, CRC Taylor & Francis Group, London, 2006.
[6] Bruni S., Vinolas J., Berg M., Polach O., Stichel S.: Modelling of suspension components in a rail vehicle dynamics context, Vehicle System Dynamics, 2011, Vol. 49, No. 7, pp. 1021-1072.
[7] Mazzola L., Alfi S., Bruni S.: The influence of modelling of the suspension components on the virtual homologation of a railway vehicle, Proceedings of the First International Conference on Railway Technology: Research, Development and Maintenance, Las Palmas de Gran Canaria, Spain, 2012, Civil-Comp Press, Stirlingshire, UK, Paper 75.
[8] Eickhoff B.M., Evans J.R., Minnis A.J.: A review of modelling methods for railway vehicle suspension components, Vehicle System Dynamics, 1995, Vol. 24, No. 6-7, pp. 469-496.
[9] Berg M.: A model for rubber springs in the dynamic analysis of rail vehicles, Proceedings of the Institution of Mechanical Engineering, Part F: Journal of Rail and Rapid Transit, 1997, Vol. 211, pp. 95-108.
[10] Berg M.: A non-linear rubber spring model for vehicle dynamics analysis, Vehicle System Dynamics, 1998, Vol. 28, pp. 723-728.
[11] Berg M.: A Non-Linear Rubber Spring Model for Rail Vehicle Dynamics Analysis, Vehicle System Dynamics, 1998, Vol. 30, pp. 197-212.
[12] Dumitriu M.: Influence of damping suspension on the vibration eigenmodes of railway vehicles, Mechanical Journal Fiability and Durability, 2013, Iss. 1, pp. 109-115.

Nieliniowy model połączenia sprężyny śrubowej i elementu gumowego w zawieszeniu pionowym pojazdu szynowego

S t r e s z c z e n i e

W artykule przedstawiono nieliniowy model reprezentujący właściwości mechaniczne połączenia sprężyny śrubowej i elementu gumowego wykorzystywanego w zawieszeniu wtórnym pasażerskiego pojazdu szynowego. Zasada modelu polega na założeniu nakładania się trzech składowych sił pochodzących od sprężystości, lepkości i tarcia suchego. W modelu są dwa źródła nieliniowości, związane odpowiednio z siłami sprężystości i tarcia. Główne atrybuty modelu uwidoczniono na podstawie jego odpowiedzi na pobudzenie harmoniczne typu przemieszczenia. Wyniki otrzymane przez zastosowanie symulacji numerycznej pokazują szereg podstawowych właściwości modelu, w tym zależność odpowiedzi modelu od amplitudy i częstotliwości pobudzenia, a także od jego sztywności i tłumienia.